Estimation of Cerebral Blood Flow From Dynamic Susceptibility Contrast MRI Using A Tissue Model

Joshua S. Shimony[1], John J. Lee[1], and G. Larry Bretthorst[2]

Mallinckrodt Institute of Radiology[1] and Department of Chemistry[2], Washington University Medical School
521 S. Kingshighway Blvd., St. Louis, MO 63110, USA

Abstract. Cerebral perfusion measurements are of great clinical and research interest. Positron emission tomography (PET) is considered the gold standard for cerebral perfusion measurement, but is not widely available and entails exposure of the subject to radioactivity. Dynamic susceptibility contrast (DSC) MRI methods are becoming more widely available on the newest generation of MRI scanners. The standard analysis methods of this data have significant disadvantages that include the use of a single, difficult to measure, arterial input function for the entire brain and the need to perform a numerical deconvolution on the logarithm of noisy data. These methods are not yet fully validated and remain qualitative in nature. Using a modification of the standard tracer kinetic principles we implemented a tissue perfusion model that has several advantages over standard methods. The model parameters were estimated using Bayes probability theory in a group of patients with varying degrees of hemodynamic impairment and were found to provide additional physiologic information that was not available using standard techniques.

Keywords: Bayes probability theory, Cerebral perfusion, MRI, Carotid occlusion.
PACS: 02.50.Cw

INTRODUCTION

The accurate measurement of cerebral perfusion remains a difficult research and clinical challenge [1]. Such a measurement could increase our understanding of normal and abnormal brain physiology. Many common disorders of the brain, such as stroke and neoplasm, manifest through perfusion abnormalities and could be better diagnosed and treated with accurate perfusion measurements.

The technique of positron emission tomography (PET) can provide quantitative values of perfusion parameters, however it is not widely available due to the need for an on-site cyclotron and entails exposure of the subject to radioactivity [2-4]. In the last several years, cerebral perfusion measurements using dynamic susceptibility contrast (DSC) MRI have become widely available on clinical scanners in the hope of overcoming these disadvantages [5]. Currently these methods are qualitative in nature and incompletely validated [6]. These measurements are performed by injecting a bolus of MRI contrast agent (Gd-DTPA) through a large bore catheter into a vein. The brain is imaged rapidly (approximately once every second) and the passage of the contrast agent is quantified by the signal intensity changes seen in the brain.

CP803, *Bayesian Inference and Maximum Entropy Methods in Science and Engineering*
edited by Kevin H. Knuth, Ali E. Abbas, Robin D. Morris, and J. Patrick Castle
© 2005 American Institute of Physics 0-7354-0292-2/05/$22.50

The analysis of DSC MRI measurements is based on the Fick principle of conservation of contrast agent in tissue [1]. This principle states that the change in the amount of contrast in the tissue is equal to the amount supplied by the arteries minus that removed by the veins. A large feeding artery is identified in the brain (usually one of the middle cerebral arteries) and the signal changes recorded in it are used to define the arterial input function (AIF) used in the standard analysis of this data [7]. The venous outflow is difficult to measure and is modeled using the tissue impulse response function.

The calculation of perfusion parameters from these measurements requires the calculation of the residue curve in each pixel of the image. This function is monotonically decreasing and expresses the fraction of remaining contrast in the pixel [8]. Traditionally, the signal data are converted into concentrations by taking their logarithm. A deconvolution, which can be unstable with noisy data, is performed between the tissue concentration curves in each pixel and the AIF [5]. The standard MRI and PET methods use a single AIF for the whole brain. However this is unlikely to be valid in patients with unilateral carotid occlusion that were evaluated in this study. A single AIF cannot account for the different delay and dispersion that occur before the bolus arrives at the capillary bed. An additional problem with the AIF measurement arises from the high concentration of contrast within the arteries during the peak of the bolus. This often causes saturation of the signal making it difficult to accurately estimate the contrast agent concentration during this period [9].

In this manuscript we propose a tissue perfusion model that allows both the AIF and residue curve to be determined for each pixel in the image. The parameters appearing in this model are estimated using Bayesian probability theory and Markov chain Monte Carlo simulations to sample the joint posterior probability for the parameters. Preliminary results using this model are superior to traditional methods and provide additional valuable perfusion parameters that are not obtainable using standard techniques.

METHODS

Experimental Data

The St. Louis Carotid Occlusion Study was a large clinical trial that investigated hemodynamics in patients with chronic cerebrovascular disease [10-13]. Both symptomatic and asymptomatic patients were enrolled and were evaluated for their risk of stroke under optimal medical management. In 19 of the patients perfusion measurements were made using both PET and MRI within one hour of each other. Written informed consent was obtained on all subjects in accordance with guidelines of the local institutional review board.

The MRI exams were performed on a 1.5T Magnetom Vision (Siemens; Erlangen, Germany). Following anatomic imaging a bolus of the contrast agent gadodiamide (Omniscan, Nycomed) was administered at a dose of 0.2 mmol/kg at a rate of 5 mL/s with a power injector through a large bore antecubital IV catheter. Just prior to and following the contrast injection, dynamic imaging was performed using a single shot

echo planar imaging technique (TR 800 ms; TE 47 ms; flip angle 60 degrees; field of view 24 cm; matrix 96 x 200) covering the brain with 8 axial sections, each of 6-mm thickness. The sequence was repeated once a second for a total of 80 s. The time series were corrected for head motion and realigned using rigid body transformations. Following the realignment procedure signal time courses were obtained for each pixel in the brain (Figure 1A). These data sets were analyzed using the model described below.

Tracer Kinetic Model

Tracer kinetic perfusion models are based on several fundamental principles [8,14,15]. The first of these is Fick's law of conservation of contrast agent in tissue. This states that the change in the concentration of contrast agent in the tissue (C_T; units mmol/mL brain) can be expressed as the cerebral blood flow (CBF; units mL blood/s·mL brain) times the concentration of contrast agent delivered by the artery (AIF or C_A; units mmol/mL blood) minus that removed by the vein (C_V; units mmol/mL blood):

$$\frac{dC_T(t)}{dt} = CBF\left[C_A(t) - C_V(t)\right]. \tag{1}$$

In the range of usual flows and concentrations the tissue response is approximately linear and the venous output concentration can be expressed as a convolution of the AIF and the tissue response function, h(t):

$$C_V(t) = C_A(t) \otimes h(t). \tag{2}$$

This substitution eliminates the venous concentration, which is difficult to measure. The formal solution to this equation with all the initial conditions set to zero is given by:

$$C_T(t) = CBF \cdot R(t) \otimes C_A(t). \tag{3}$$

R(t) is the pixel residue curve which is a function of the pixel response function:

$$R(t) = 1 - \int_0^t h(t')dt'. \tag{4}$$

This residue curve is defined to be 1.0 at time zero, and then monotonically decreases. It represents the fraction of remaining contrast in the tissue over time.

The central volume rule is another fundamental principle used in tracer kinetics models. Basic to this principle is the concept of mean transit time (MTT) in the tissue. The assumption is that the blood delivered by an artery to a capillary bed will be split into smaller units that will traverse through capillaries of different length and spend a different amount of time in the tissue. The MTT is determined by the CBF and the cerebral blood volume (CBV) of the tracer:

$$MTT = \frac{CBV}{CBF}. \tag{5}$$

Using this principle the perfusion parameters can be calculated from the residue curve in each pixel. Since the residue curve is multiplied by the CBF, its non-normalized value at the bolus arrival time is proportional to the CBF and the area

under the normalized curve is the MTT. The CBV can then be derived using the central volume principle.

Additions to the Standard Model

Several modifications were made to the previously presented standard tracer kinetic model. The contrast agent concentration was converted to a signal intensity measured in the MRI experiment:

$$S(t) = S_0 \exp[-kC_T(t)], \tag{6}$$

with k being a constant that depends on the experimental echo time. Additionally we selected an exponential form for the residue function, with δ being the wash-out constant, the inverse of the MTT:

$$R(t) = \exp[-\delta(t - t_0)] = \exp[-(t - t_0)/MTT]. \tag{7}$$

This residue curve decrease monotonically and has other required features (equal to 1 at t=0 and has a normalized area of MTT). Also, this functional form is the one theoretically derived for a tracer that can diffuse to the extra-vascular volume [14,15]. More complex functional forms may be needed to describe the data in the case of non-diffusable tracers such as Gd-DTPA. We initially used an exponential multiplied by a polynomial in powers of $(t-t_0)$. However, given the quality of the data, including these extras terms did not significantly reduce the estimate of the standard deviation of the noise, and, consequently, were not used in the following analysis.

The signal curve (Figure 1A) has three distinct components. The large initial dip arises from the arrival of the main contrast bolus in the tissue. The second, smaller, delayed dip, represents the re-circulation of the main bolus after passing through the right heart, lungs, left heart, and back to the brain. Finally, the last component needs to account for the difference in baseline of the signal before and after the administration of contrast. This difference arises from the steady state distribution of the contrast agent in blood.

Both the primary and secondary bolus of contrast was modeled using a normalized gamma-variate function. Gamma-variate functions are often used for this purpose in the physiology literature [16]:

$$GV(t, t_0) = \frac{\beta^{\alpha+1}}{\Gamma(\alpha+1)}(t - t_0)^{\alpha} \exp[-\beta(t - t_0)]. \tag{8}$$

Given the signal to noise ratio in our data we could not differentiate between the parameters α and β in the primary and secondary boluses. The difference between the primary and secondary bolus was expressed as a difference in the area under the curves and in different arrival times (t_0 and t_1). The baseline steady state difference was expressed as an additive constant giving the following expression for the AIF:

$$C_A(t) = aGV(t, t_0) + bGV(t, t_1) + c. \tag{9}$$

These expressions were substituted into equation Eq. [3] and the convolution was performed analytically.

Bayesian Inference and Markov chain Monte Carlo

The posterior probabilities for the model parameters were computed for each pixel given the time series data using Bayesian probability theory [17]. There are a total of ten parameters, expressed as a group by the Greek letter Ω. Two of the parameters are the traditional perfusion parameters CBF and the wash-out constant δ=1/MTT. The next two parameters express the primary and re-circulation bolus arrival times, t_0 and t_1. The shape of the arriving bolus was described by the gamma-variate parameters α and β. Finally, the remaining parameters express the baseline signal, S_0, and the relative size of the terms in the AIF (a,b, and c in Eq. [9]). Bayes' theorem states that the posterior probability for the parameters, given the data D and the relevant background information I, can be expressed as a product of the direct probability for the data and the prior probabilities for the model parameters:

$$P(\Omega|DI) \propto P(D|\Omega, I)P(\Omega|I). \tag{10}$$

The prior probability was factored into independent prior probabilities for each parameter:

$$P(\Omega|I) \propto P(CBF|I)P(\delta|I)P(\alpha|I)P(\beta|I)P(t_0|I)\ldots(Q)^{-N/2}. \tag{11}$$

All of the prior probabilities were assigned using Gaussian prior probabilities bounded by an appropriate physiologic range. The likelihood, $P(D|\Omega,I)$, was assigned using a Gaussian noise prior probability. The standard deviation of this prior was removed by marginalization using a Jeffreys' prior, resulting in the Student's t-distribution (on the right of Eq. [11]). The total square residual (Q) was given by:

$$Q = \sum_i [D_i - S(t_i)]^2, \tag{12}$$

with D_i being the measured signal data items. The joint posterior probability was sampled using a Metropolis-Hastings Markov chain Monte Carlo simulation with simulated annealing [18,19].

RESULTS

An example of the model estimate of the signal in a single pixel is presented in Figure 1B. The original data is presented in blue, with the estimate in green. The model demonstrates a reasonable estimate of the data with a small residual shown in red.

Parameter estimates were performed in a patient determined to be hemodynamically normal based on PET measurements. No differences were seen between the left and right side in any of the parameter maps, confirming the fact that this patient has normal collateral circulation in the brain despite having a unilateral carotid occlusion.

Parameter estimates in a patient with left hemodynamic impairment are presented in Figures 2 and 3. Figure 2A, B, and C demonstrates single slice maps of the CBF, δ=1/MTT, and CBV respectively. The CBF map appears symmetric, however asymmetry is seen between the left side of the brain, which is hemodynamically compromised, and the right side in the wash-out parameter, δ (smaller on the left side)

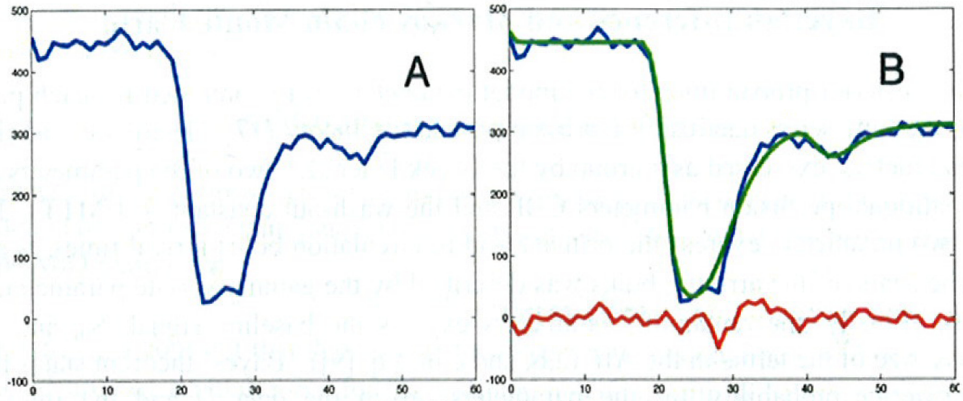


FIGURE 1: (A) Signal intensity versus time (blue) during the passage of the contrast bolus in a single pixel. (B) Model estimation of the signal intensity (green) and the estimation residue (red).

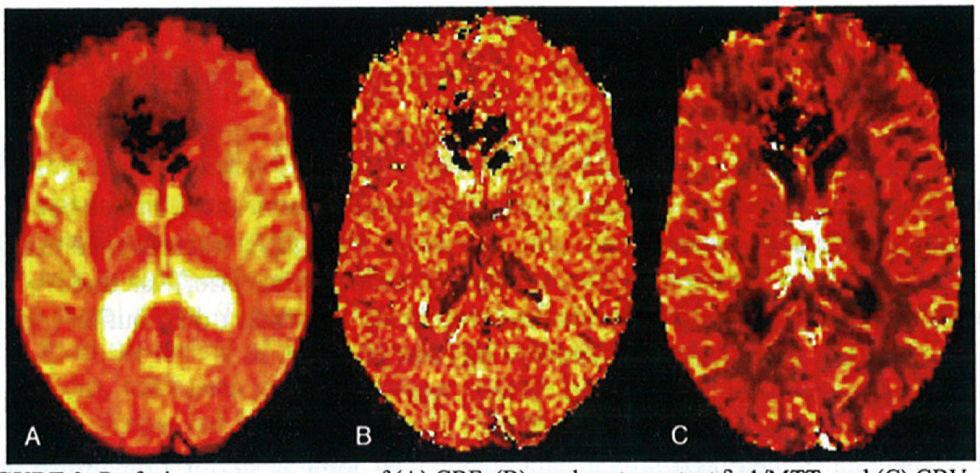


FIGURE 2: Perfusion parameter maps of (A) CBF, (B) wash-out constant δ=1/MTT, and (C) CBV. Asymmetry between the left and right side of the brain is seen in (B) and (C). Images are in an arbitrary scale white>yellow>red. Model parameter estimates are not accurate in the ventricles.

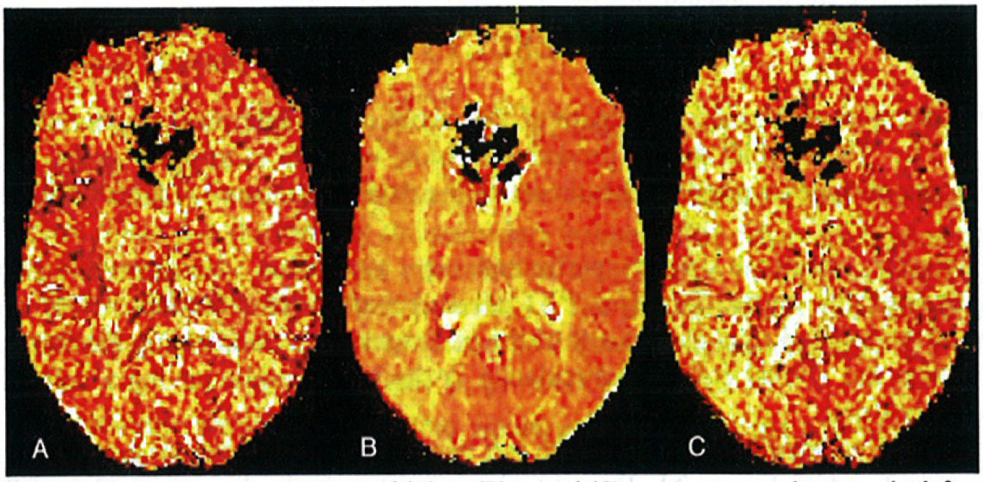


FIGURE 3: Perfusion parameter maps of (A) α, (B) t_0, and (C) t_1. Asymmetry between the left and right side of the brain is seen in all images. Images are in an arbitrary scale white>yellow>red. Model parameter estimates are not accurate in the ventricles.

and CBV (longer on the left side). Evaluation of perfusion in this patient using standard MRI techniques did not demonstrate this hemodynamic impairment. Figure 3A demonstrates asymmetry between the left and right side of the brain in the gamma-variate parameter α, which is smaller on the left as compared to the right. This finding represents a slower rise time of the contrast bolus, as would be expected from collateral supply. Similarly, Figures 3B and 3C show asymmetry between left and right in the primary and secondary bolus arrival time, which is longer on the left. This finding is also consistent with delay in supply on the left due to indirect flow in the collateral circulation. The model parameter estimation is designed for brain tissue and is not accurate for points external to the brain, which were masked out, nor are they accurate in the ventricles, which have no blood flow within them.

SUMMARY

Current methods of measuring perfusion parameters using DSC MRI have significant disadvantages that include taking the logarithm of the data prior to analysis, using a single AIF that cannot account for different delay and dispersion in different parts of the brain, difficulty in measuring this AIF reliably due to saturation effects, and relying on deconvolution of noisy data. These systemic problems can seriously bias the measured values [20-22].

Preliminary data presented above indicate that pixel-by-pixel perfusion model parameter estimation based on Bayesian inference is able to overcome many disadvantages of current methods. Many of the model parameters are unique to this method and could provide important physiological information not available using current techniques. Further analysis of this data in a larger sample of patients and comparison with the PET data is planned for future study.

ACKNOWLEDGEMENTS

We would like to thank W. J. Powers, C. P. Derdeyn, and T. O. Videen for the use of the St. Louis Carotid Occlusion Study data. We would like to thank A. Z. Snyder for help in performing the image realignment.

REFERENCES

1. Siesjo BK. Brain Energy Metabolism. New York: John Wiley and Sons, 1978.
2. Raichle ME. Positron Emission Tomography. *Ann. Rev. Neurosci.* 1983; 6:249-267.
3. Powers WJ, Raichle ME. Positron Emission Tomography and its application to the study of cerebrovascular disease in man. *Stroke* 1985; 16:361-375.
4. Powers WJ, Zazulia AR. The use of Positron Emission Tomography in cerebrovascular disease. *Neuroimag. Clin. N. Am.* 2003; 13:741-758.
5. Ostergaard L, Weisskoff RM, Chesler DA, Gyldensted C, Rosen BR. High resolution measurement of cerebral blood flow using intravascular tracer bolus passages. Part I: Mathematical approach and statistical analysis. *Magn. Res. Med.* 1996; 36:715-725.
6. Powers WJ, Zivin J. Magnetic resonance imaging in acute stroke: not ready for prime time. *Neurology* 1998; 50:842-3.
7. Sorensen AG, Reimer P. Cerebral MR Perfusion Imaging. Berlin: Thieme, 2000.

8. Zierler KL. Theoretical basis of indicator-dilution methods for measuring flow and volume. *Circulation Research* 1962; 10:393-407.
9. Akbudak E, Conturo TE. Arterial input functions from MR phase imaging. *Magn. Res. Med.* 1996; 36:809-815.
10. Powers WJ, Press GA, Grubb RL, Gado M, Raichle ME. The effect of hemodynamically significant carotid artery disease on the hemodynamic status of the cerebral circulation. *Ann. Int. Med.* 1987; 106:27-35.
11. Grubb RL, Derdeyn CP, Fritsch SM. Importance of hemodynamic factors in the prognosis of symptomatic carotid occlusion. *JAMA* 1998; 280:1055-1060.
12. Derdeyn CP, Grubb RL, Powers WJ. Cerebral hemodynamic impairment: methods of measurement and association with stroke risk. *Neurology* 1999; 53:251-259.
13. Derdeyn CP, Videen TO, Yundt KD. Variability of cerebral blood volulme and oxygen extraction: stages of cerebral hemodynamic impairment revisited. *Brain* 2002; 125:595-607.
14. Von Schulthess GK, Hennig J. Functional Imaging. Philadelphia: Lippincott-Raven, 1998.
15. Zazulia AR, Markham J, Powers WJ. Cerebral blood flow and metabolism in human cerebrovascular disease. In: Mohr JP, ed. Stroke: Pathophysiology, Diagnosis, and Management: Churchill and Livingstone, 2004.
16. Miles K, Dawson P, Blomley M. Functional Computed Tomorgraphy. Oxford: Oxford University Press, 1997.
17. Jaynes ET. Probability Theory: the logic of science. In: Bretthorst GL, ed. Cambridge: Cambridge University Press, 2003.
18. Metropolis N, Rosenbluth AW, Rosenbluth MN, Teller AH, Teller E. Equations of state calculations by fast computing machines. *J. Chem. Phys.* 1953; 21:1087-1091.
19. Gilkes WR, Richardson S, Spiegelhalter DJ. Markov Chain Monte Carlo in Practice. London: Chapman and Hall, 1996.
20. Calamante F, Gadian DG, Connelly A. Delay and dispersion effects in dynamic susceptibility contrast MRI: simulations using singular value decomposition. *Magn. Res. Med.* 2000; 44:466-473.
21. Calamante F, Gadian DG, Connelly A. Quantification of perfusion using bolus tracking MRI in stroke: assumptions, limitations, and potential implications for clinical use. *Stroke* 2002; 33:1146-1151.
22. Wu O, Ostergaard L, Koroshetz WJ, Schwamm LH, O'Donnell J, Schaefer PW, Rosen BR, Weisskoff RM, Sorensen AG. Effects of tracer arrival time on flow estimates in MR perfusion weighted imaging. *Magn. Res. Med.* 2003; 50:856-864.